


Nanoscale vacuum channel transistor with in-plane collection structure

Ji Xu^{1,3} , Hai Hu^{2,3}, Wenxin Yang¹ , Chi Li^{2,4}, Yutong Shi¹, Yongjiao Shi¹, Qilong Wang^{1,4} and Xiaobing Zhang^{1,4}

¹ Joint International Research Laboratory of Information Display and Visualization, Southeast University, Nanjing 210096, People's Republic of China

² Division of Nanophotonics, CAS Center for Excellence in Nanoscience, National Center for Nanoscience and Technology, Beijing 100190, People's Republic of China

E-mail: lichi@nanocr.cn, northrockwq1@seu.edu.cn and bell@seu.edu.cn

Abstract

High quality nanoscale vacuum channel transistors (NVCTs) enable carriers to transport ballistically through the vacuum nanogap, achieving high speed and frequency characteristic which are essential for on-chip vacuum electronic devices. However, the studies to date have been largely confined to explore the common electrical performance, while the fast response characteristic of NVCTs remains a challenge. We report the fabrication of metal-based NVCT, with sub-100 nm vacuum channel and specific designed in-plane collection structure which can enhance the emission or collection efficiency of the electrons simultaneously. Importantly, the demonstration of a rise/fall time of less than 100 ns is achieved, which is compatible with those high-quality solid-state transistors based on low-dimensional materials. Moreover, the device can also retain excellent electrical performance, exhibiting a high drive current ($>10 \mu\text{A}$), low work voltage ($<10 \text{ V}$) and high on/off current ratio ($>10^4$). The verification of fast temporal response of NVCT makes a significant step towards on-chip vacuum electronics with high speed and integration.

Keywords: nanoscale vacuum channel, vacuum transistor, in-plane collection structure, fast temporal response

1. Introduction

Vacuum electronics initiated and promoted the early development of electronics, e.g. signal amplification or modulation, was mostly based on traditional vacuum tubes [1]. Numerous studies have focused on the development of vacuum electronics such as thermionic [2–4] or cold [5–7] field emission devices, which plays an important role in the fields of aerospace, communications and medication [8]. In order to match the current integrated electronic device usage environment, however, there is an essential need to develop vacuum

devices down to nanoscale level. As vacuum is intrinsically superior to semiconductor owing to the transport medium, carries are able to transmit more easily through a vacuum channel while suffering collisions inside the crystal lattice of solid-state device. The velocity of electrons can accelerate far beyond over $5 \times 10^7 \text{ cm s}^{-1}$ in silicon, achieving high-speed eventually. In this case, with a vacuum channel less than 100 nm or even the mean-free-path of electrons, ballistic transport may occur in the nanoscale vacuum that enables significantly high switching speed, low operating voltage and power consumption.

As a result, researchers have proposed the nanoscale vacuum channel transistor (NVCT) [9–11] or vacuum field effect transistor (FET) [12–14] as an alternative method to

³ Ji Xu and Hai Hu contributed equally to this work.

⁴ Authors to whom any correspondence should be addressed.

realize the concept of vacuum-on-chip devices [15, 16]. Composed of vacuum nanogap as carriers transport channel and low-function materials as cold cathode, NVCT facilitates electrons to transport ballistically inside the vacuum channel that expected to acquire outstanding electrical properties [17–19]. Despite NVCTs have made fast progress in recent years, there are still some practical issues to be solved. On the one hand, both of the capacity of emitting electrons and collection efficiency are restricted by the conventional tip-to-tip structure. For instance, the output current of present NVCTs is merely in the order of nanoamps for metal [20] and graphene-based devices [10], which may be a limiting factor for practical applications such as x-ray tubes [21], electron sources [22] or high-power microwave devices [23]. On the other hand, the studies to date have been largely confined to explore the common electrical performance, while the fast response characteristic of NVCTs remains as a challenge [24]. Previous theoretical and simulated results have both found that the transit time of electrons may achieve the magnitude of nanosecond in a sub-100 nm vacuum channel, which significantly reveal the intrinsic superiority of NVCT [25, 26]. However, the experimental efforts of the temporal response for NVCT still stays in the microsecond level, that may be the hinder for future practical applications.

To this end, a metal-based NVCT is demonstrated with specific designed in-plane collection structure in order to achieve high output current and fast temporal response. Compared to the conventional tip-to-tip structure, our in-plane collection structure can dramatically enhance the capacity and efficiency of emitting/collecting electrons. The states of our device can be modulated by applying a back-gate voltage, showing remarkable performance of high drive current ($>10\ \mu\text{A}$), low work voltage ($<10\ \text{V}$) and high on/off current ratio ($>10^4$). Importantly, we further present the demonstration of a turn-on/off time less than 100 ns for a sub-100 nm vacuum channel, which is compatible with reported FETs based on graphene or other low-dimensional materials. The designed in-plane collection structure can achieve fast temporal response, high output current and more importantly the feasibility of high integration, indicating the potential in the concept of vacuum-on-chip devices for NVCTs.

2. Experimental

The influence factors of high output current may attribute to two main reasons: (I) capacity of emitting electrons, which is related to the electric field intensity and (II) the efficiency of collecting electrons. It is noted that previous reports show current limitations ($<1\ \mu\text{A}$) of metal-based NVCT, which is not applicable in practical devices [20, 27]. In order to improve the output current by enhancing the emission/collection efficiency, simulations are carried out to investigate the influence of collector structure on the electron transport trajectory and electrical field distribution, as is shown in the supplementary information, available online at stacks.iop.org/NANO/31/065202/mmedia. Figure 1(a) exhibits the

electric field distribution of different structure and the peak field intensity normalized by the value of the single-terminal as collector is shown in figure 1(b). The maximum local field was extracted from the simulation results for comparisons, that a local field enhancement of 38% can be acquired by the three-terminals structure. On the other hand, the emission current is in direct ratio with the number of electrons reaching the collector. In terms of geometry, the collection efficiency of three-terminals structure shows a 17% growth of the collected electrons, as is shown in figure S1. Both simulation results of the field distribution and electron trajectory suggest that the three-terminals structure can lead to effective current increase. Importantly, the proposed device structure can be readily fabricated by conventional semiconductor process that may be viewed as an alternative approach for NVCT.

As a result, the three-terminal NVCT is fabricated according to the simulation results. Figure 1(c) shows the schematic diagram of the proposed metal-based NVCT. The vacuum nano-channel was fabricated with combination of electron beam lithography (EBL), thin film deposition and lift-off process. Firstly, silicon dioxide (SiO_2) was thermally grown on highly n-doped silicon, with a thickness of 300 nm. After spin-coating PMMA (poly (methyl methacrylate)) on the precleaned substrate, the nanogap was defined by standard EBL (Vistec, EBPG 5000plus ES). Then, a 60 nm Au layer was deposited by electron beam evaporation with 5 nm Cr as adhesion layer. With a subsequent lift-off process, the vacuum nanoscale channel was formed, as is shown in figure 1(d). Also, the structure was processed via 1 h of annealing at 400°C in the quartz tube with the flow of hydrogen (70 sccm) and argon (40 sccm), strengthening the gold nanoribbons in order to avoid melt down of high current. A zoomed-in view of the vacuum nano-channel is depicted in figure 1(e).

3. Results and discussion

3.1. Electrical performance

After the preparation of the three-terminals structure, the current–voltage (I – V) characteristics are measured in a vacuum chamber (~ 10 – $2\ \text{Pa}$). Figure S2 exhibits the digital photography of the prepared device after bonding. The output (I_c – V_c curves) and transfer characteristics of the metal-based NVCT are shown in figures 2(a) and (b), respectively. Similar to the typical FETs, the metal-based NVCT could be switched in off- or on-state by the gate voltage. As is shown in figure 2(a), it can be seen that no obvious emission current I_c was measured when V_g is less than the threshold voltage (off-state). As the V_g increases, the NVCT switches to the on-state that I_c exhibit an exponentially growth with collector voltage V_c . We note that the NVCT exhibits a drive current as high as the order of $10\ \mu\text{A}$, which is about two orders of magnitude higher than previous metal-based devices. The high drive current of the NVCT is attributed to the three-terminal collectors, that dramatically improve the efficiency of emitting/collecting

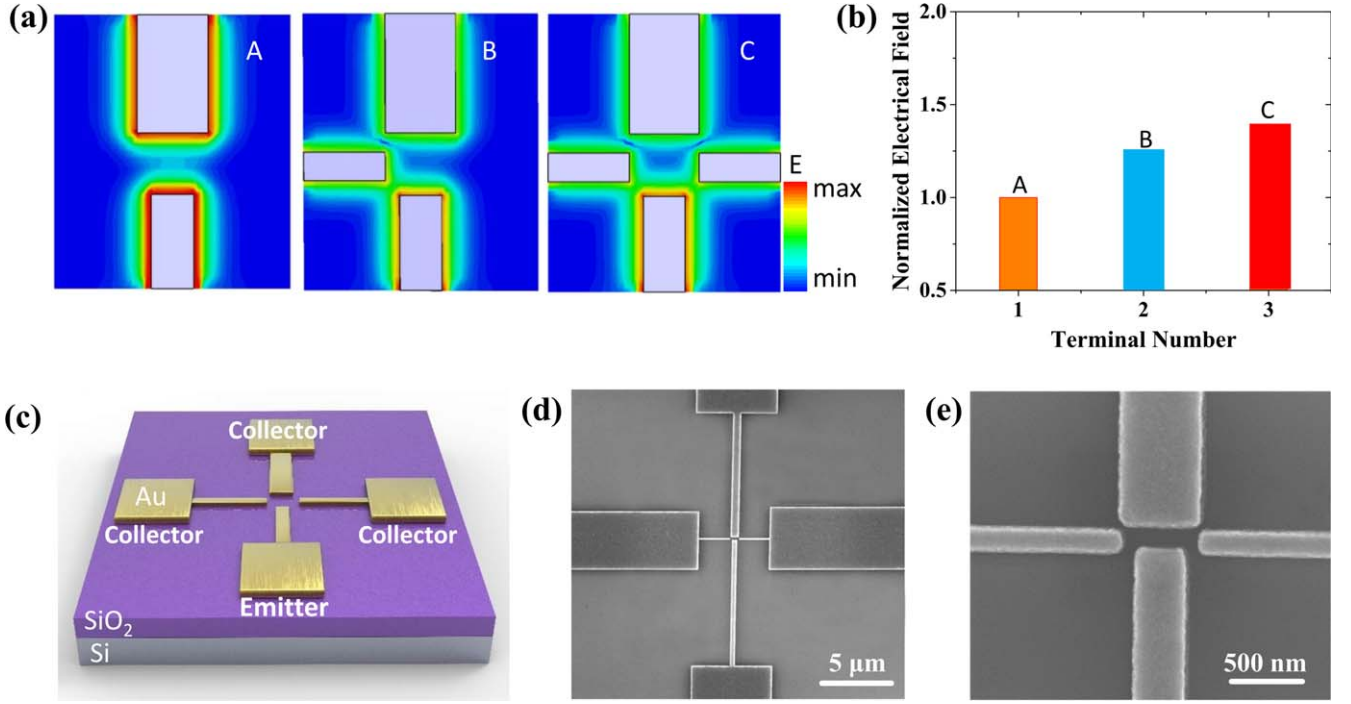


Figure 1. (a) Electric field distribution of different vacuum nanogap structures. (b) Peak field intensity normalized by the value of single-terminal as collector. (c) Schematic diagram of the proposed metal-based NVCT. (d) Top view of SEM image of the NVCT. (e) Zoomed-in view of the vacuum nanoscale channel.

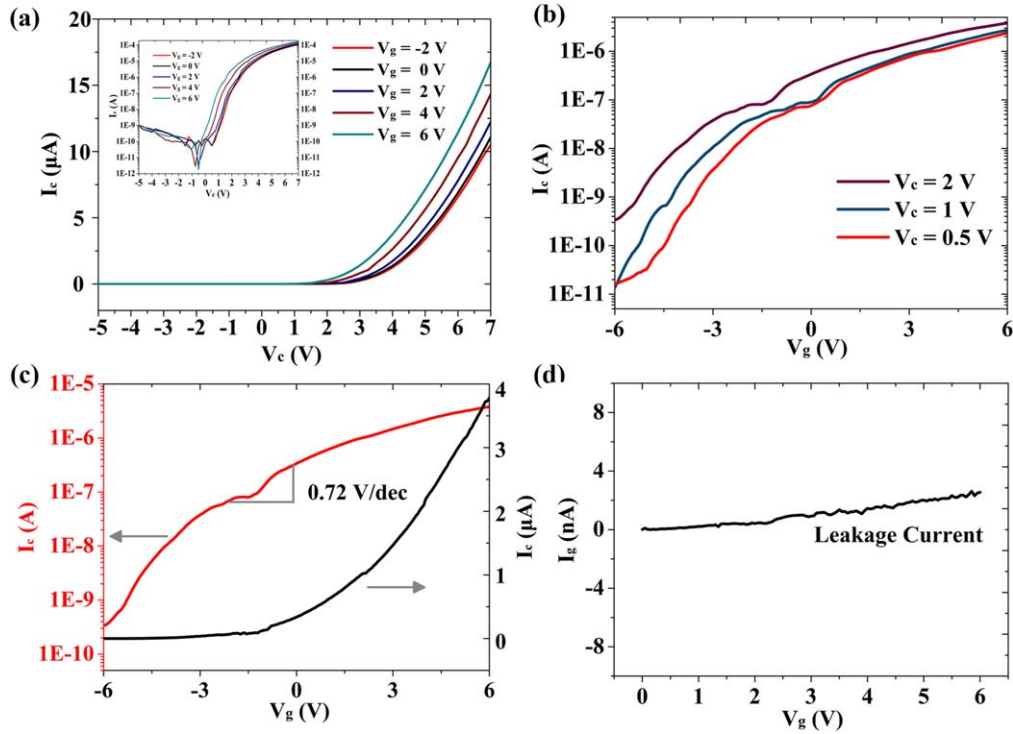


Figure 2. (a) Output characteristic (I_c - V_c curves) corresponding to gate voltage increases from -2 to 6 V at 2 V intervals. The inset shows the I_c - V_c curves in semilog scale. (b) Transfer characteristic (I_c - V_g curves) plotted in exponential scale. (c) Transfer characteristic of the NVCT when $V_c = 2$ V, showing an on/off current ratio up to 10^4 . (d) Leakage current (I_g - V_g curve) of the NVCT.

electrons. Moreover, the inset shows the I_c - V_c curves in semi-log scale. We observe that our device also demonstrates a current rectifying behavior that can be understood by the simulations, as is shown in figure S3. It is noted that the

emitting electrons present crossed trajectories under a reverse bias, thus showing a conventional diode-like behavior. Figure 2(b) illustrates the transfer characteristics in exponential scale with different V_c . The I_c - V_g plots indicate that I_c increases

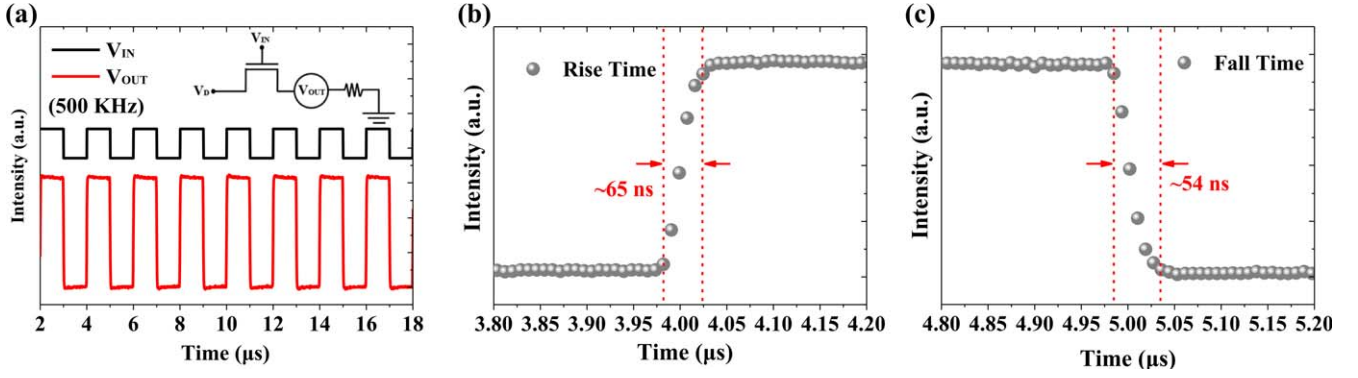


Figure 3. (a) Temporal response of the emission current turned on/off with the frequency of 500 KHz. A single normalized cycle for estimating the detailed (b) rise and (c) fall time, respectively. The rise/fall time was defined as increased/decreased from 10%/90% to 90%/10% of the stable current.

exponentially with V_g with an on/off current ratio as high as 10^4 obtained.

Figure 2(c) illustrates the transfer characteristic with $V_c = 2$ V in liner (black line) and exponential (red line) scale, respectively. The electrons could be drawn from the emitter with a positive gate voltage. The curves plotted in exponential scale exhibit an on/off current ratio exceeding 10^4 due to the small off-state current (<0.1 nA), and the subthreshold slope is 0.72 V/dec. The high on/off current ratio and low subthreshold slope shows that our device possesses excellent modulation capability that strongly related with the gate structure. For the three-terminals NVCT, the emission current is modulated by the back-gate structure, in which the insulator plays a crucial role in the device. We further detect the leakage current during the measurement, as is shown in figure 2(d). The gate leakage current is less than 5 nA, which is 10^4 times smaller than the emission current. However, the back-gate structures usually show an inevitable compromise between the gate controllability and the insulator thickness. A thin insulating layer could enhance the modulation ability of back-gate while the insulator should be thick enough to acquire negligible leakage current. The performance of NVCT is declined by this trade-off effect. We suggest that high-k materials could be utilized, e.g. Al_2O_3 or HfO_2 , to avoid breakdown with thinner insulators while enhancing modulation ability simultaneously.

3.2. Temporal response measurement

Response speed is also a critical parameter of an electron device, which signifies the capability to follow a rapidly signal. Meanwhile, it still lacks of the experimental efforts of the temporal response for NVCT, which cannot reveal the intrinsic superiority of the nanoscale vacuum channel. Thus, we also study the temporal response of the proposed three-terminals NVCT. The response speed of the metal-based NVCT in this study is evaluated by an oscilloscope and the input voltage is generated by a signal generator. Figure 3(a) shows the output signal of the NVCT corresponding to a square wave signal. We note that our device exhibits excellent switching characteristic with a fast response frequency of 500 KHz and good reproducibility.

Furthermore, a single normalized cycle for estimating the detailed rise and fall time are illustrated in figures 3(b) and (c), respectively. Here the rise/fall time is determined as the time it takes for the output voltage increase from 10%(90%) to 90%(10%) upon a change of input voltage. Notably, it can be seen that the rise and fall time is 65 and 54 ns, illustrating the demonstration of NVCT with temporal response in sub-100 ns time scale. For comparison, the experimental efforts on the thermionic NVCT as electron source still stays in the microsecond level as the emission current is driven by the thermal effect. This result can further verify the advantage of ultra-fast initiation for field emission applications, compared with traditional bulky thermionic emitters. On the other hand, the sub-100 ns temporal response exhibits the essential quality of NVCT, showing its great potentials in high-speed applications.

In addition, the fast response measurement under pulse with the frequency of 500 KHz, 1 MHz, 5 MHz and 10 MHz are carried out (figure S4), and the values of rise/fall time with error bar is illustrated in figure 4, respectively. Under the square wave signal, our device could demonstrate switching performance with fast response and good reproducibility for frequencies of 500 KHz, 1 MHz and 5 MHz, that the on/off current ratios still remain consistent with the increasing frequency. With the frequency reaching up to 10 MHz, however, the output of NVCT cannot achieve the maximum when the input is off, as is shown in figure S4. The upper limit of response time may be ascribed mainly to the modulation capacity of the gate, that further optimizing the overlap between gate contacts and emitter/collector could accelerate the response speed. Nonetheless, it is worth noting that the response time of our device is not inferior to the reported FETs or NVCTs based on low-dimensional materials, including carbon nanotubes (CNTs), graphene or TMDCs (table 1).

3.3. Comparison of solid-state transistors and NVCTs

To compare the performance of our device with those typical solid-state transistors and NVCTs, the aspects of operating voltage, on/off ratio, subthreshold swing and response time are listed in table 1. For these reported solid-state transistors,

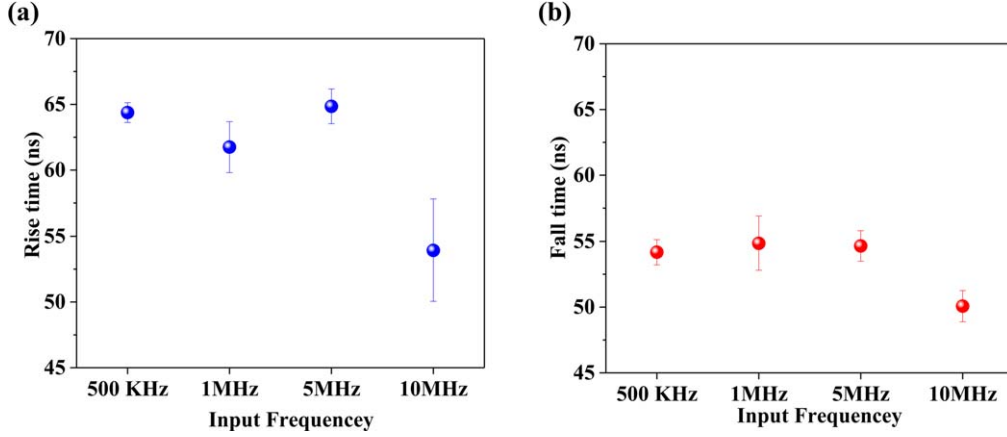


Figure 4. (a) The rise time and (b) fall time under square wave signal with the input frequency of 500 KHz, 1 MHz, 5 MHz and 10 MHz, respectively.

Table 1. Comparison of solid-state transistors and NVCTs.

Device	Operating voltage (V)	On/off ratio	Subthreshold swing (mV/dec)	Response time (ns)	References
CNT TFT	<3 V	$\sim 10^5$	—	1200	[28]
SWCNT/ZTO TFT	<5 V	2.6×10^7	—	140	[29]
Gr-based FET	<5 V	$\sim 10^6$	210	—	[30]
MoS ₂ transistor	<5 V	$\sim 10^7$	—	0.58	[31]
Si-based NVCT	<15 V	10^6	4200	—	[15]
Gr-based NVCT	<15 V	$\sim 10^6$	120	<1000	[10]
Metal-based NVCT	<5 V	$\sim 10^3$	—	—	[20]
This paper	<10 V	1.5×10^5	720	68	

the carriers transport from the source to the drain through the low-dimensional material channel, following the drift and diffusion mechanism. We can find that all the high-quality solid-state transistors can demonstrate low operating voltages (<5 V), high on/off ratio ($>10^5$) and low subthreshold swing (<500 mV/dec), whereas the response time vary from each other. Printed thin film transistor (TFT) based on CNTs were demonstrated to exhibit excellent switching characteristics with on/off ratio of 10^5 with supply voltage below 3 V, while the response time still remains in the order of microsecond [28]. In addition to bare CNT TFTs, Kim *et al* selected zinc tin oxide (ZTO) as the active semiconductor due to its high mobility, that the hybrid TFTs could perform an ultra-high on/off ratio of 2.6×10^7 with response time of 140 ns [29]. FETs based on sub-10 nm wide graphene nanoribbons reported the best electrical performances among all intrinsic graphene-based solid-state transistors with an on/off current ratio up to 10^6 and a subthreshold swing of 210 mV/dec [30]. Transition metal dichalcogenides (TMDCs) can also be utilized in high-speed transistors. Duan and co-workers reported the state-of-art MoS₂ transistor, achieving a response time less than 1 ns [31]. By comparing the electrical properties, it is worth noting that the performance of our NVCT is not far behind from those high-quality solid-state transistors based on low-dimensional materials, showing the potential of NVCT in high-speed and low cost applications.

Similarly, for NVCTs composed of other materials and structure, electrons tunnel from the emitters and travel

ballistically in the vacuum channel when the gate voltage is beyond the threshold. Many efforts have already been made to downscale the width of vacuum channel and realize the on-chip vacuum transistors. To our knowledge, the first demonstration of NVCT was by Meyyappan *et al* in 2012 with standard silicon semiconductor processing [15]. The back-gate NVCT based on silicon were reported have an on/off ratio up to 10^6 , whereas with a high operating voltage of 15 V and a large subthreshold slope of 4200 mV/dec. Nirantar *et al* presented the all-metal NVCT with channel less than mean-free-path in air (68 nm), which could enable devices to function with low operating voltage (<5 V) in air medium, but only a low on/off ratio of 10^3 was experimentally demonstrated [20]. On the other hand, low-dimensional materials such as graphene could also be utilized as the field emitters. Wei *et al* exhibit the graphene-based NVCT with on/off current ratio up to 10^6 and a subthreshold slope of 120 mV/dec [10]. These results demonstrate that NVCT could combine the advantages of both solid-state and vacuum electronics with low power consumption and high integration. Meanwhile, the experimental efforts of the temporal response for NVCT are rather deficient, compared to the solid-state transistors. Apart from the comparable values of operating voltages (<10 V), on/off ratio ($>10^5$) and subthreshold swing (~ 720 mV/dec), our devices present the demonstration of the response time less than 100 ns, which may overturn the stereotype that vacuum devices are inferior to the solid-state devices.

In general, the high speed response performance may mainly attribute to the essential feature of the vacuum channel, that the velocity of electrons may be accelerated with minimal collision or scattering, traveling ballistically from emitters to collectors. Moreover, the conspicuous advantage of vacuum devices is their capacity of functioning under extreme environment with less degradation than the solid-state devices [19]. Meyyappan *et al* have fabricated a surround-gate NVCT and the device was proved to operate normally under the ionizing radiation (proton and Gamma ray) or high temperature conditions (200 °C) [9]. Nonetheless, a straight comparison between solid-state and vacuum nanoelectronics of their electrical performance and reliability is scarce. We hope that it could be presented in a future publication, demonstrating that vacuum-on-chip devices are vital and superior to CMOS in specific areas. However, an obvious shortage of all the NVCTs is the large supply voltage and a subsequent high electrical field that motivates the field emission. Due to the intense electrical field at the emitters, the accumulated Joule heating may limit the speed of NVCTs. In addition, the power efficiency is also a concerned problem as the high working voltage up to tens of volts. Further improvement may be derived from emitters with low work function materials or structure optimization such as device downscaling and geometry engineering [7, 32–37]. Besides, the substrate may be the main limiting factor for the transportation for lateral-type NVCTs. Generally, the NVCTs consists of two categories, lateral- and vertical-type. For vertical-type NVCTs, the emitters are perpendicularly fabricated on the substrate, e.g. CNTs or SiC, that electrons can freely travel through the vacuum channel without scattering or collisions from the substrate. In lateral-type devices, on the other hand, the emitters and collectors are usually fabricated in the same plane of the substrate surface. The noticeable advantage for lateral devices lies in the design freedom, that the structure parameters such as gap-spacings or electrode shapes can be simply achieved by layout variation. However, with current flowing horizontally, the electrons would inevitably suffer backscattering or collisions from the substrate. Han *et al* suggested that a surround-gate structure can be utilized in the lateral NVCTs, rather than back- or bottom-gate, providing the best electrostatic control of transport in the vacuum channel [38]. It may be an alternative approach to solve the limiting factors of the substrate.

3.4. Theoretical discussion

Different from the drift-diffusion mechanism of solid-state transistors, the carrier transport in the vacuum nano-channel is dominated by the tunneling process. Figure 5(a) shows the band diagram of NVCT switches from off-state to on-state with increasing gate voltage. When the gate voltage is less than the threshold voltage, only a few electrons could overcome the broad barrier due to the thermal energy. Meanwhile, the width of the barrier can be compressed with the increasing gate voltage. As the gate voltage increases beyond the threshold voltage, the electrons could overcome the narrowed barrier via F–N tunneling, leading to the on-state of the NVCT.

In order to further explain these experimental results, we resort to basic tunneling model and semiconductor theory. It is crucial to determine the tunneling mechanism that NVCT follows, so that the I – V curves need to be examined and redraw to fit the established models. The classic Fowler–Nordheim (F–N) tunneling theory [39, 40] can be expressed by the following equation

$$I_{FN} = A(\beta^2 V_C^2 / \Phi d^2) \exp(-B \Phi^{3/2} d / \beta V_C), \quad (1)$$

where $A = 1.56 \times 10^{-6}$ ($A \text{ V}^{-2} \text{ eV}$) and $B = 6.83 \times 10^9$ ($V \text{ eV}^{-3/2} \text{ V m}^{-1}$) are constants, I is the emission current, β is the field enhancement factor related to the materials and emitter geometry, Φ is the work function (eV), d is the distance between the emitter and collector, and V is the applied voltage. By taking the logarithm of both sides, equation (1) turns into

$$\ln(I_{FN} / V_C^2) = \ln(a) - b(1/V_C) \quad (2)$$

in which the linearity tendency of $\ln(I/V^2)$ versus $1/V$ testifies that F–N tunneling mechanism is dominated for carriers transportation.

Hence, the F–N plots for I_C – V_C curve with $V_g = 2 \text{ V}$ in figure 5(b) illustrates that our device agrees with the F–N theory, and the field enhancement β of 4193.7 is acquired by calculation according to equation (1). Meanwhile, an up-bending trend is noted at low supply voltage regime. Meyyappan *et al* suggested that this phenomenon may attribute to the protrusion of the emitter that creating more possible emitting spots [9, 41]. However, the variation of the slope indicates that the emission efficiency becomes poor along with the decreasing electric field. According to the band diagram, we suppose that the current emission at low operating voltage is related with Schottky emission by thermal effect. With an applied bias, the energy barrier is lowered by the image force, which is called the Schottky effect. As the barrier width is too broad to tunneling, that only few electrons may overcome the energy barrier at the metal-vacuum interface, due to the thermal energy. The Schottky emission can be expressed as [42]

$$I_{\text{Schottky}} = AT^2 \exp(\Phi - \beta V_C^{1/2} / kT), \quad (3)$$

where A is the effective Richardson constant, T is the temperature, β is the dielectric constant, k is the Boltzman's constant. By taking the logarithm of both sides, the plots of $\ln I_C$ versus $V_C^{1/2}$ will appear as a straight line at a constant T . As a result, we extract the I – V plots at low bias and redraw it in the form of $\ln I_C$ versus $V_C^{1/2}$, as is shown in figure 5(c). Obviously, the linearity conforms the Schottky emission in our device with low supply voltage. Besides, the low current emission may also attribute to the tunneling electrons in SiO_2 layer which conforms to the Frenkel–Poole (F–P) transport. Di Bartolomeo *et al* suggested that the electrons may be injected in the trapping states of the oxide for F–P model [43]. In this case, the tunneling electrons can move in a sequence of trapping states, leading to the reduction of the barrier. As a result, combining the above analysis, it is assumed that only a few of high-energy electrons may ‘climb’ over the broad vacuum barrier or tunneling through the oxide layer in low

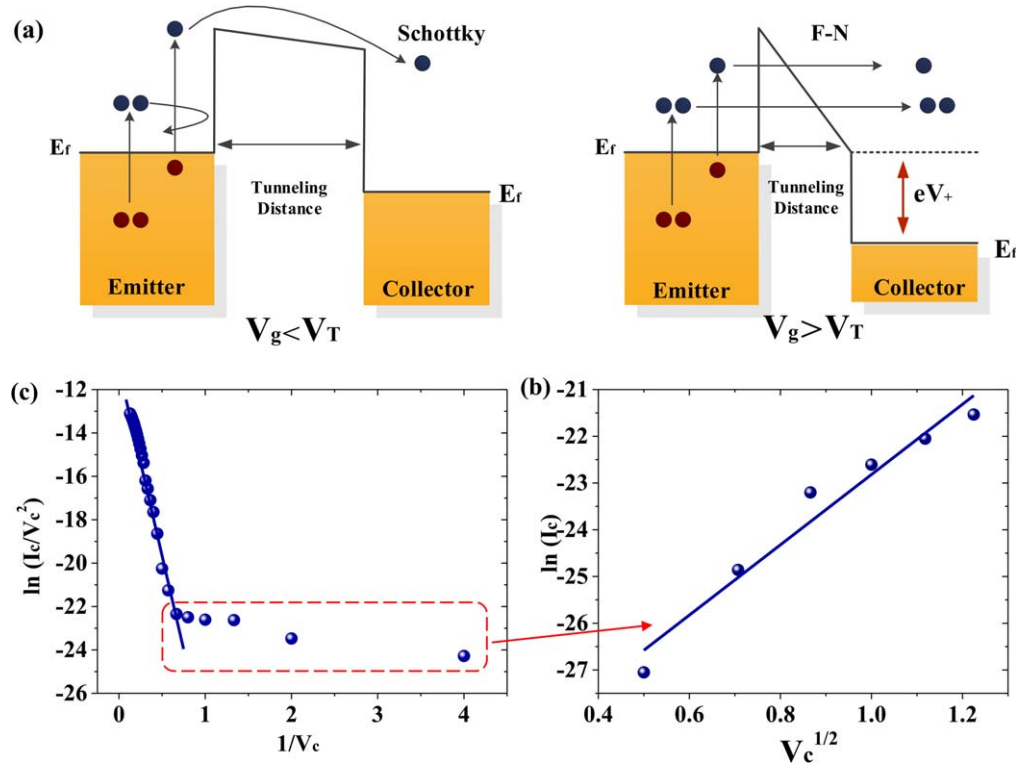


Figure 5. (a) Band diagram of the metal-based NVCT in off and on-state. (b) Fowler–Nordheim plots for I_c – V_c curve with $V_g = 2$ V. (c) Schottky emission characteristic for I_c – V_c curve in low working voltage regime.

working voltage regime. As the electric field further increases, F–N theory becomes the dominating factor that a dramatically increasing emission current can be detected.

4. Conclusions

In summary, a metal-based NVCT is successfully fabricated by standard CMOS process. With the specially designed three-terminals structure, emission/collection efficiency are improved to obtain high emission current. Importantly, we further present a turn-on/off time less than 100 ns for the NVCT, which is far superior to proposed thermionic or cold field emission NVCTs. By modulating the back-gate voltage, the NVCT could be switched from off-state to on-state, exhibiting an on/off current ratio up to 10^4 with high drive current ($>10 \mu\text{A}$) and low working voltages (<10 V). Furthermore, basic tunneling model is utilized to explain the experimental results. We note that F–N tunneling is dominant at high electric field, while the current emission at low operating voltage is related with Schottky emission by thermal effect. The fast temporal response and capacity of high integration indicate the potential of NVCT in high speed and low cost applications.

Acknowledgments

This work is financially supported by the China Postdoctoral Science Foundation (2019M651646), the National Natural

Science Foundation of China (61904029, 61571124 and 61971133), the National Basic Key Research Program of China (Grant No. 2015CB932400), the National Key Research and Development Program of China (Grant No. 2016YFA0201600).

Conflicts of interest

There are no conflicts to declare.

References

- [1] Brinkman W F, Haggan D E and Troutman W W 1997 A history of the invention of the transistor and where it will lead us *IEEE J. Solid-State Circuits* **32** 1858–65
- [2] Jensen K L and Cahay M 2006 General thermal-field emission equation *Appl. Phys. Lett.* **88** 154105
- [3] Kan M C, Huang J L, Sung J C, Chen K H and Yau B S 2003 Thermionic emission of amorphous diamond and field emission of carbon nanotubes *Carbon* **41** 2839–45
- [4] Garguilo J M, Koeck F A M, Nemanich R J, Xiao X C, Carlisle J A and Auciello O 2005 Thermionic field emission from nanocrystalline diamond-coated silicon tip arrays *Phys. Rev. B* **72** 165404

- [5] Spindt C A 1968 A thin-film field-emission cathode *J. Appl. Phys.* **39** 3504
- [6] Spindt C A, Holland C E, Rosengreen A and Brodie I 1991 Field-emitter arrays for vacuum microelectronics *IEEE Trans. Electron Devices* **38** 2355–63
- [7] Wu Z S, Pei S F, Ren W C, Tang D M, Gao L B, Liu B L, Li F, Liu C and Cheng H M 2009 Field emission of single-layer graphene films prepared by electrophoretic deposition *Adv. Mater.* **21** 1756
- [8] Granatstein V L, Parker R K and Armstrong C M 1999 Vacuum electronics at the dawn of the twenty-first century *Proc. IEEE* **87** 702–16
- [9] Han J-W, Moon D-I and Meyyappan M 2017 Nanoscale vacuum channel transistor *Nano Lett.* **17** 2146–51
- [10] Wu G, Wei X, Zhang Z, Chen Q and Peng L 2015 A graphene-based vacuum transistor with a high ON/OFF current ratio *Adv. Funct. Mater.* **25** 5972–8
- [11] Xu J, Gu Z, Yang W, Wang Q and Zhang X 2018 Graphene-based nanoscale vacuum channel transistor *Nanoscale Res. Lett.* **13** 311
- [12] Huu Duy N, Kang J S, Li M and Hu Y 2019 High-performance field emission based on nanostructured tin selenide for nanoscale vacuum transistors *Nanoscale* **11** 3129–37
- [13] Wang X, Shen Z H, Wu S L and Zhang J T 2017 Vacuum field-effect transistor with a deep submicron channel fabricated by electro-forming *Solid-State Electron.* **132** 1–5
- [14] Hu B H, Yazdanpanah M M, Kane B E, Hwang E H and Das Sarma S 2015 Strongly metallic electron and hole 2D transport in an ambipolar Si-vacuum field effect transistor *Phys. Rev. Lett.* **115** 036801
- [15] Han J-W, Oh J S and Meyyappan M 2012 Vacuum nanoelectronics: back to the future?—Gate insulated nanoscale vacuum channel transistor *Appl. Phys. Lett.* **100** 213505
- [16] Srisophonphan S, Jung Y S and Kim H K 2012 Metal-oxide-semiconductor field-effect transistor with a vacuum channel *Nat. Nanotechnol.* **7** 504–8
- [17] Gaertner G 2012 Historical development and future trends of vacuum electronics *J. Vac. Sci. Technol. B* **30** 060801
- [18] Utsumi T 1991 Vacuum microelectronics—whats new and exciting—keynote address *IEEE Trans. Electron Devices* **38** 2276–83
- [19] Dodd P E, Shaneyfelt M R, Schwank J R and Felix J A 2010 Current and future challenges in radiation effects on CMOS electronics *IEEE Trans. Nucl. Sci.* **57** 1747–63
- [20] Nirantar S, Ahmed T, Ren G, Gutruf P, Xu C, Bhaskaran M, Walia S and Sriram S 2018 Metal-air transistors: semiconductor-free field-emission air-channel nanoelectronics *Nano Lett.* **18** 7478–84
- [21] Sugie H, Tanemura M, Filip V, Iwata K, Takahashi K and Okuyama F 2001 Carbon nanotubes as electron source in an x-ray tube *Appl. Phys. Lett.* **78** 2578–80
- [22] Zhang H, Tang J, Yuan J S, Yamauchi Y, Suzuki T T, Shinya N, Nakajima K and Qin L C 2016 An ultrabright and monochromatic electron point source made of a LaB₆ nanowire *Nat. Nanotechnol.* **11** 273
- [23] Field M et al 2018 Development of a 100-W 200-GHz high bandwidth mm-wave amplifier *IEEE Trans. Electron Devices* **65** 2122–8
- [24] Wu G, Wei X, Gao S, Chen Q and Peng L 2016 Tunable graphene micro-emitters with fast temporal response and controllable electron emission *Nat. Commun.* **7** 11513
- [25] Zhu Y B, Zhang P, Valfells A, Ang L K and Lau Y Y 2013 Novel scaling laws for the Langmuir–Blodgett solutions in cylindrical and spherical diodes *Phys. Rev. Lett.* **110** 5
- [26] Xu J, Wang Q L, Qi Z Y, Zhai Y S and Zhang X B 2015 Study on the frequency characteristics of nanogap electron devices *J. Appl. Phys.* **117** 204504
- [27] Xu J, Wang Q, Tao Z, Zhai Y, Chen G, Qi Z and Zhang X 2017 High-quality and stable electron emission device with Sub-30-nm aligned nanogap arrays *IEEE Trans. Electron Devices* **64** 2364–8
- [28] Ha M J, Seo J W T, Prabhumirashi P L, Zhang W, Geier M L, Renn M J, Kim C H, Hersam M C and Frisbie C D 2013 Aerosol jet printed, low voltage, electrolyte gated carbon nanotube ring oscillators with sub-5 μ s stage delays *Nano Lett.* **13** 954–60
- [29] Kim B, Jang S, Geier M L, Prabhumirashi P L, Hersam M C and Dodabalapur A 2014 High-speed, inkjet-printed carbon nanotube/zinc tin oxide hybrid complementary ring oscillators *Nano Lett.* **14** 3683–7
- [30] Wang X R, Ouyang Y J, Li X L, Wang H L, Guo J and Dai H J 2008 Room-temperature all-semiconducting sub-10nm graphene nanoribbon field-effect transistors *Phys. Rev. Lett.* **100** 206803
- [31] Cheng R, Jiang S, Chen Y, Liu Y, Weiss N, Cheng H C, Wu H, Huang Y and Duan X F 2014 Few-layer molybdenum disulfide transistors and circuits for high-speed flexible electronics *Nat. Commun.* **5** 5143
- [32] Ye D X, Moussa S, Ferguson J D, Baski A A and El-Shall M S 2012 Highly efficient electron field emission from graphene oxide sheets supported by nickel nanotip arrays *Nano Lett.* **12** 1265–8
- [33] Late D J, Shaikh P A, Khare R, Kashid R V, Chaudhary M, More M A and Ogale S B 2014 Pulsed laser-deposited MoS₂ thin films on W and Si: field emission and photoresponse studies *ACS Appl. Mater. Interfaces* **6** 15881–8
- [34] Koh A L, Gidcum E, Zhou O and Sinclair R 2016 The dissipation of field emitting carbon nanotubes in an oxygen environment as revealed by *in situ* transmission electron microscopy *Nanoscale* **8** 16405–15
- [35] Chen L F, Yu H, Zhong J S, Song L H, Wu J and Su W T 2017 Graphene field emitters: a review of fabrication, characterization and properties *Mater. Sci. Eng. B* **220** 44–58
- [36] Pescini L, Tilke A, Blick R H, Lorenz H, Kotthaus J P, Eberhardt W and Kern D 2001 Nanoscale lateral field-emission triode operating at atmospheric pressure *Adv. Mater.* **13** 1780–3
- [37] Park I J, Jeon S G and Shin C 2014 A new slit-type vacuum-channel transistor *IEEE Trans. Electron Devices* **61** 4186–91
- [38] Han J-W, Seol M-L, Moon D-I, Hunter G and Meyyappan M 2019 Nanoscale vacuum channel transistors fabricated on silicon carbide wafers *Nat. Electron.* **2** 405–11
- [39] Lenzlinger M and Snow E H 1969 Fowler–Nordheim tunneling into thermally grown SiO₂ *J. Appl. Phys.* **40** 278
- [40] Ellis R K 1982 Fowler–Nordheim emission from nonplanar surfaces *Electron Device Lett.* **3** 330–2
- [41] de Assis T A, Dall’Agnol F F and Andrade R F S 2016 The consequences of dependence between the formal area efficiency and the macroscopic electric field on linearity behavior in Fowler–Nordheim plots *J. Phys. D: Appl. Phys.* **49** 35
- [42] Odwyer J J 1966 Current-voltage characteristics of dielectric films *J. Appl. Phys.* **37** 599
- [43] Di Bartolomeo A, Giubileo F, Iemmo L, Romeo F, Russo S, Unal S, Passacantando M, Grossi V and Cucolo A M 2016 Leakage and field emission in side-gate graphene field effect transistors *Appl. Phys. Lett.* **109** 023510